Optical absorption and photoluminescence in pristine and photopolymerized C_{60} solid films

Ying Wang,* J. M. Holden, A. M. Rao, and P. C. Eklund†
Department of Physics and Astronomy, University of Kentucky, Lexington, Kentucky 40506

U. D. Venkateswaran
Department of Physics, Oakland University, Rochester, Michigan 48309

DeLyle Eastwood and Russell L. Lidberg‡
Lockheed Environmental Systems and Technologies Company, Las Vegas, Nevada 89119

G. Dresselhaus
Francis Bitter National Magnet Laboratory, Massachusetts Institute of Technology, Cambridge, Massachusetts 02139

M.S. Dresselhaus
Department of Electrical Engineering and Computer Science and Department of Physics, Massachusetts Institute of Technology, Cambridge, Massachusetts 02139
(Received 20 June 1994)

The optical absorption (OA) and photoluminescence (PL) spectra of pristine, oxygen-free C_{60} films in the vicinity of the absorption edge across the highest-occupied-molecular-orbital to lowest-unoccupied-molecular-orbital (HOMO-LUMO) gap are studied to elucidate the nature of these electronic states. Structures observed in both the OA and PL spectra are identified with Herzberg-Teller vibronic coupling of the respective singlet electronic states to intramolecular vibrational modes. Similarities and differences among the PL and OA spectra of C_{60} in solution, solid films, and single crystals are discussed. The larger linewidth of the C_{60} film spectra is attributed to the presence of defects, presumably associated with numerous grain boundaries. Finally, the OA and PL spectra of photopolymerized C_{60} solid films are presented. The features in both the OA and PL spectra are observed to broaden considerably. In addition, two of the OA bands blueshift slightly (400–800 cm^{-1}) and the PL features downshift by $\sim$330 cm^{-1} upon photo-polymerization. These results are consistent with the intermolecular oligomerization bond disorder and reduced symmetry of the C_{60} shell imposed by the covalent bonds between C_{60} molecules in the polymeric phase.

I. INTRODUCTION

The optical absorption (OA) and photoluminescence (PL) spectra of C_{60} molecules in solution have been intensively studied.[1–4] At the absorption edge ($\sim$1.9 eV for C_{60} molecules[1]), the optical transitions between electronic states should be parity forbidden because of the icosahedral symmetry of the molecule. However, with sufficient electron-vibrational coupling to modes of appropriate symmetry, the oscillator strength can become large enough to activate these parity-forbidden transitions. Thus, sharp features observed near the absorption edge in the OA and PL spectra of C_{60} in solution[3,4] have been identified with transitions between Herzberg-Teller (HT) vibronic states based on a many-electron molecular electronic state coupled to an ungerade intramolecular vibration of appropriate symmetry.[1,2,5]

In the solid fcc phase, HT coupling, as well as intermolecular interactions, are both expected to affect the nature of the optical transitions in the ultraviolet-visible (UV-vis) range. Ching et al.,[6] for example, have calculated the optical dielectric function $\epsilon(0,\omega)$ for solid

C_{60}, and they find important contributions to $\epsilon(0,\omega)$ from transitions between the h_u-derived valence band and the t_{1u}-derived conduction band. Despite the fact that wave-vector conserving (or "vertical") transitions between these bands are forbidden at both the Γ and X points in the Brillouin zone, transitions between these bands at other points in the zone are found in this calculation to contribute significant oscillator strength. In the work of Ching et al.,[6] it was not necessary to invoke an electron-phonon coupling (nonvertical transitions), or HT coupling, to activate electric-dipole transitions between h_u- and t_{1u}-derived energy bands.

In more recent calculations on the solid state optical properties of C_{60}, Louie and co-workers[7] stress that the electron-hole interaction is very large and gives rise to a series of Frenkel exciton bands deep in the gap between the h_u- and t_{1u}-derived bands. They have calculated that the lowest exciton energy is 1.6 eV, approximately 0.4 eV below the t_{1u}-derived conduction band edge. The optical threshold of solid C_{60} is seen experimentally near $\sim$1.7 eV,[8,9] and according to Louie and co-workers, this absorption is due to the electric-dipole excitation of this

lowest excitonic state, which they find to be strongly localized on a single molecule. Furthermore, they contend that band gap values of 2.3–2.6 eV reported in photoemission experiments[10–12] are in accord with the calculated gap (2.0 eV) between the quasiparticle valence and conduction states.

Since second-order IR[13] and Raman scattering[14] spectra of solid C_{60} exhibit sharp overtone and combination lines, it is clear that crystalline C_{60} is a nearly ideal molecular solid. It still remains an interesting question, however, as to what extent the intermolecular interactions lead to a breakdown in the molecular optical selection rules. Indeed, some authors have proposed an altogether opposite view of solid C_{60}, viz., that crystalline C_{60} is a one-electron, bandlike semiconductor,[15] and they have calculated the electronic contribution to the dielectric function in this limit. In fact, solid C_{60} may be best described by models that lie somewhere in between these extreme points of view, as proposed recently by Louie[7] and Harigaya.[16]

In this paper, we make a correspondence between the assignment of the features observed in the PL and OA spectra of C_{60} solid films with those observed in C_{60} solutions based on the many-electron molecular picture. Near the optical threshold, or "optical band gap," the remarkable similarities between film and solution spectra lead us to conclude that the vibronic transitions have the same origin for both thin film and solution samples. Recently, Guss *et al.*[17] have assigned the features in the PL spectrum of their C_{60} single crystals to overlapping contributions from C_{60} molecules located in different crystalline environments, i.e., to the presence of so-called X traps. In the first part of this paper, we compare the vibronic features in the PL and OA spectra of C_{60} in solution to that of a thin solid film prepared by vacuum sublimation, and our PL data with that from a single crystal reported by Guss *et al.*[17]

Since early workers[18] reported problems in obtaining spot-to-spot reproducibility in the PL spectra of C_{60} solid films, we have carried out OA and PL measurements of pristine, oxygen-free solid C_{60} films from the same spot, and with low excitation intensity. From our previous studies,[19,20] the lack of spot-to-spot reproducibility[18] in the PL spectra is probably associated with the photosensitivity of solid C_{60}.[20] We have shown that pristine solid C_{60}, in the absence of molecular oxygen, undergoes a phototransformation when exposed to visible or ultraviolet light.[19–21] Experimental evidence for this phototransformation includes measurements by laser desorption mass spectroscopy,[20,21] changes in the solubility of C_{60} films in organic solvents,[20] UV-vis absorption spectroscopy,[20] Raman spectroscopy,[19,20,22–24] infrared spectroscopy,[20] and photoelectron spectroscopy.[25] As in previous studies,[22–24] Raman lines were used to characterize the sample before and after phototransformation, because the Raman-active, polarized mode at 1469 cm^{-1} (pristine, fcc C_{60}) is sensitive to the degree of photopolymerization of the film, with the frequency of this $A_g(2)$ mode downshifting to 1458 cm^{-1} in phototransformed films.[26] PL and OA spectra obtained for photopolymerized C_{60} are also discussed in this paper.

II. EXPERIMENTAL DETAILS

A. C_{60} solid films

Both OA and PL experiments in the vicinity of the optical absorption edge (1.8 eV) were carried out on the same spot of solid C_{60} films ($\sim$4500 Å thick), using the apparatus shown schematically in Fig. 1. Light traversed the double-grating spectrometer (Spex Model No. 1680) in the forward direction (solid lines) for acquiring optical absorption spectra using light from a tungsten lamp. The PL spectrum was analyzed using the same spectrometer in the reverse direction (dashed lines). The PL excitation was accomplished with the 488 nm line of an argon ion laser at a power density of 0.06 W/cm^2 to minimize the degree of photopolymerization of pristine C_{60}. Both the quartz lens (labeled SL3 in Fig. 1) and the sample were fixed in position. For the PL measurements, a cylindrical lens (CL) was used to illuminate approximately the same rectangular area (spot size $\sim$1 $\times$ 5 mm^2) as was used in the OA experiments. The light intensity was detected by a GaAs photomultiplier tube (RCA No. 4832). For the PL and OA experiments, the sample was in vacuum and was thermally anchored to a copper cold finger of an evacuated cryostat. The sample temperature was monitored by a Au-Fe thermocouple, attached by silver epoxy to the front surface of the fused silica substrate (Suprasil).
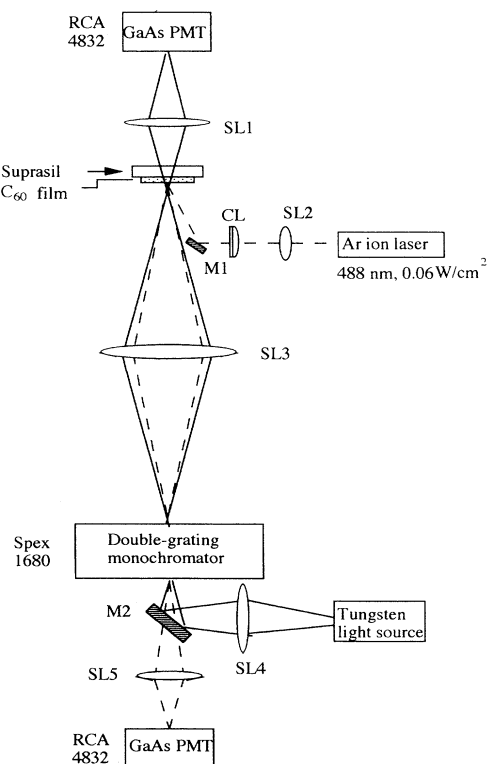

FIG. 1. Optical apparatus for measurement of the PL and OA spectra of solid C_{60} films. Both spectra were taken on the same spot on the film (see text). Solid and broken lines denote the optical paths for OA and PL measurements, respectively.

The room temperature transmittance measurements of thinner solid C_{60} films ($\sim$500 Å) in the energy range 0.5–6 eV were made using a prism spectrometer (Perkin Elmer Model No. 83).

C_{60} films (both $\sim$4500 Å and $\sim$500 Å thick) were deposited on Suprasil substrates by vacuum sublimation of microcrystalline C_{60} powder. Details concerning the sample preparation and film thickness determination are reported elsewhere.[20] After deposition, the $\sim$4500-Å-thick C_{60} films were transferred quickly (1–2 min) under flowing N_2 gas to the optical cryostat which was then immediately evacuated to $\sim$10^{-4} Torr. The $\sim$500-Å-thick C_{60} films were transferred into a rectangular quartz tube inside the He glovebox containing the deposition chamber, and then evacuated to $\sim$10^{-7} Torr and sealed. Phototransformed films were prepared by placing the pristine C_{60} films encapsulated in rectangular quartz ampoules at the focal point of a quartz lens, which converged UV-vis broad band light from a 500 W mercury lamp. These C_{60} films were checked for their degree of phototransformation before and after each OA or PL spectrum was taken by measuring the relative intensity of the Raman lines at 1469 and 1458 cm^{-1}. The sample was judged to be completely transformed when no Raman line was observed at 1469 cm^{-1}.

B. C_{60} in solution

A Spex Fluorolog-2 spectrofluorometer was used to collect UV-vis fluorescence spectra for C_{60} solutions in spectral grade methylcyclohexane (MCH). Bandpasses used for the emission spectra were typically 8 or 4 nm for the excitation monochromator, and 4, 2, or 1 nm for the emission monochromator. The fluorescence spectra were not corrected for instrumental efficiency because of uncertainties in the correction factor at wavelengths longer than 700 nm. Absorption spectra of the C_{60} solutions were collected using a Perkin Elmer Lambda 9 spectrophotometer.

Powdered samples of C_{60} purified by gel permeation liquid chromatography[27] were dissolved and diluted to weak concentrations (approximately 6.6 $\times$ 10^{-5} M) in spectroquality MCH from Aldrich Chemical Co. The MCH solvent was selected largely because it is known to form a clear organic glass at 77 K, and also because it is a good solvent for polycyclic aromatic hydrocarbons. The UV-vis absorption was measured for C_{60} in MCH solution at room temperature with a 1-cm fluorescence-free cuvette. The emission of the C_{60} samples in solid solution, contained in a fluorescence-free Suprasil fused silica tube (3 mm i.d. was measured at 77 K in the liquid nitrogen Dewar with the emitted light collected at 90° to the exciting light.

III. RESULTS AND DISCUSSION

A. Vibronic transitions in C_{60} molecules

Figure 2 shows a schematic diagram of the lowest molecular energy levels of an isolated C_{60} molecule. The horizontal solid and dashed lines represent electronic and vibronic states, respectively, and the vertical dashed lines with arrows represent optical transitions (arrow up: absorption; arrow down: emission). Since the vibronic states are electronic states coupled to vibrational modes, a manifold of vibronic states associated with each electronic state lies above the zero-vibration electronic energy levels by an integral number of vibrational energy quanta. Light absorption or emission at $E_{0,0'}$ should be very weak, since optical electric-dipole transitions between the zero-vibration electronic states (solid vertical line with arrows at both ends) are symmetry forbidden. The quantity $E_{0,0'}$ in Fig. 2 refers to the energy difference between zero-vibration initial (0) and final (0') states which both have the same parity. A small amount of light absorption or emission at $E_{0,0'} = \hbar\omega$ occurs, however, due to defects (or solvent interactions) which lower the symmetry, especially in the case of a highly symmetric molecule such as icosahedral C_{60}, where selection rules are expected to be well obeyed. The electron-molecular vibration interaction for both the OA and PL transitions gives rise to energy differences between vibronic energy states ($E_{0,0'} - \hbar\omega_{vib}$) for the photoluminescence process, and ($E_{0,0'} + \hbar\omega_{vib}$) for the absorption process (see Fig. 2). The PL and OA transitions occur for those ω_{vib} modes that are associated with HT coupling between the initial and final electronic states involved in the particular electric-dipole transition. Since the spatial depen-
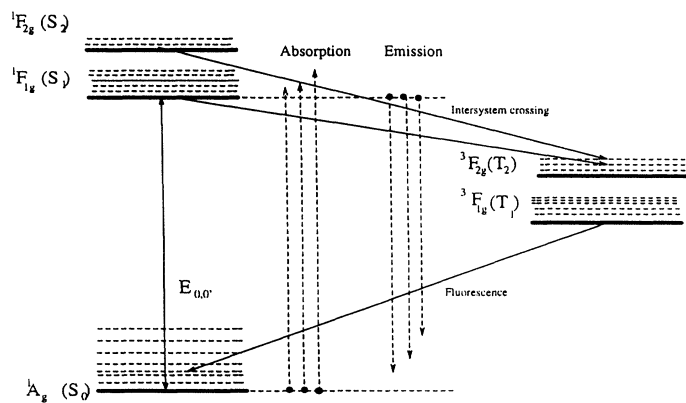

FIG. 2. Schematic energy level diagram of vibronic states (horizontal lines). Vertical arrows show the vibronic transitions between the ^1A_g ground state and various excited singlet states (e.g., $^1F_{1g}$, $^1F_{2g}$) and triplet states (e.g., $^3F_{1g}$, $^3F_{2g}$) for both the absorption and luminescence. $E_{0,0'}$ denotes the HOMO-LUMO gap.

dence of the potential $V(r)$ differs for the ground and excited states, the value for $\hbar\omega_{vib}$ in the excited states may differ slightly from that of the ground state. In the absence of an interaction between a C_{60} molecule with surrounding C_{60} or solvent molecules, the energy $E_{0,0'}$ for the noninteracting C_{60} molecules can be found at the average position of the vibronic features in the PL and OA spectra originating from the same vibrational mode $(\hbar\omega_{vib})$.

In a many-electron molecular picture, the lowest excited electronic state has the electronic configuration $h_u^9 f_{1u}^1$, which forms both singlet and triplet excitonic energy levels with symmetries: $^1F_{1g}$, $^1F_{2g}$, ^1G_g, and ^1H_g; and $^3F_{1g}$, $^3F_{2g}$, ^3G_g, and ^3H_g, respectively. The ground state has a filled level configuration h_u^{10} which is associated with the fully symmetric ^1A_g state, with singlet $S = 0$ spin. Allowed electric-dipole transitions between vibronic states based on the ^1A_g ground state and excited many-electron states can be determined by group theory. In Table I we list the symmetries of the intramolecular vibrational modes which induce transitions between the various excited singlet electronic states and the singlet ground state (^1A_g). From the table, it can be seen, for example, that the PL transition $(^1F_g; 0)\rightarrow(^1A_g; A_u)$ is allowed, where the first and second symmetry labels identifying a particular vibronic state refer, respectively, to the electronic and vibrational parts; the zero in the vibronic state $(^1F_g; 0)$ indicates that the initial state contains no vibrational quantum. The symmetry-equivalent OA transition is $(^1A_g; 0)\rightarrow(^1F_g; A_u)$, and since there is only one A_u vibrational mode, the energy of this transition is unique. The dashed vertical arrows in Fig. 2 show schematically absorption and emission transitions between ^1A_g and $^1F_{1g}$ electronic levels.

Theoretical calculations, using the "quantum mechanical extension of the consistent force field method to π-electron systems" by Negri et al.[28] have predicted that the excited triplet states ($^3F_{2g}$ and $^3F_{1g}$) lie below the two lowest excited singlet states ($^1F_{2g}$ and $^1F_{1g}$), as shown in Fig. 2. These singlet states are found to be quasidegenerate, with an energy difference of ~0.03 eV (~250 cm^{-1}). Magnetic circular dichroism experiments by Gasyna et al.[29] on C_{60} isolated in Ar matrices have unambiguously identified the vibronic features in the absorption spectrum near the absorption edge with ^1A_g

manifold to $^1F_{1g}$ manifold transitions. Features due to the transitions from the ^1A_g ground state to the $^1F_{2g}$ excited vibronic states were not observed in this experiment. Based on these results, Negri et al.[1] concluded that the $^1F_{1g}$ level lies lower in energy than the $^1F_{2g}$ level and they have also calculated the oscillator strengths for a variety of transitions involving the HT active vibrational modes using the "complete neglect of differential overlap for spectroscopy" method.[1] Furthermore, they have used their calculated results to assign the features in the room temperature OA observed by Leach et al.[3] and the 77-K PL spectrum of Wang[4] for C_{60} in solution. According to their assignment, the OA spectrum is associated with transitions from the ^1A_g ground electronic state to the $^1F_{1g}$ vibronic manifold of the lowest-unoccupied-molecular orbital (LUMO) excitonic states (i.e., $^1A_g \rightarrow {}^1F_{1g}$). Similarly, the PL spectrum is associated with radiative transitions from the $^1F_{1g}$ zero-vibration electronic state to the ^1A_g vibronic manifold of highest-occupied-molecular orbital (HOMO) states (i.e., $^1F_{1g} \rightarrow {}^1A_g$). Negri et al.[1] did not assign any vibronic features in the spectra to transitions involving the quasidegenerate $^1F_{2g}$ level, even though their calculations predict that these vibronic states also make an important contribution to the spectrum.
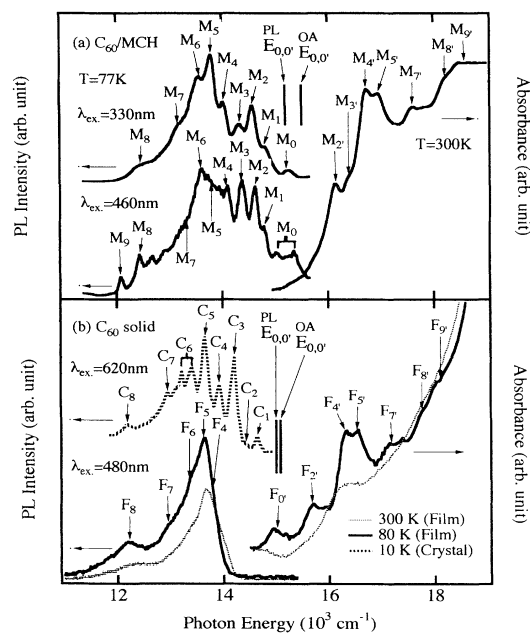
Figure 3(a) shows our room temperature (~300-K)

FIG. 3. (a) PL and OA spectra of C_{60} in 6.6×10^{-6} molar MCH solution (features labeled M_i for the PL spectra and M_i' for the OA spectra). The PL spectra were taken with 330 nm (top) and 460 nm (bottom) excitation, respectively. (b) PL (features labeled F_j) and OA (features labeled $F_{j'}$) spectra at 80 K for oxygen-free pristine ~4500-Å-thick C_{60} films on a Suprasil (fused silica) substrate. The PL excitation wavelength was 488 nm at ~ 0.06 W/cm^2. The upper curve is the 10-K PL spectrum of C_{60} single crystal (features labeled C_i) taken from Guss et al. (Ref. 17).

TABLE I. Group theoretical selection rules for vibronic transitions.

$E_{excited}$[a]	Γ_{vib}[b]
$^1F_{1g}$	A_u, F_{1u}, H_u
$^1F_{2g}$	G_u, H_u
^1G_g	F_{2u}, G_u, H_u
^1H_g	F_{1u}, F_{2u}, G_u, H_u

[a]Symmetry of the excited electronic (exciton) state.
[b]Symmetry of the vibrational mode which is involved in the HT transition. The number of modes for each symmetry type is indicated in parentheses $A_u(1)$, $F_{1u}(4)$, $F_{2u}(5)$, $G_u(6)$, and $H_u(7)$, and each of these 23 odd parity mode frequencies have different energies.

OA and 77-K PL spectra of C_{60} in a 6.6×10^{-5} molar MCH solution. The PL spectra in the spectral range $11\,700$ cm^{-1} – $16\,000$ cm^{-1} taken with excitation wavelengths of 460 nm and 330 nm are displayed, respectively, as the bottom and the top traces in Fig. 3(a). The OA spectrum for the same solution, also shown at the right in this figure, is displayed in the wavelength range between $15\,000$ cm^{-1} and $18\,500$ cm^{-1}. The features in the PL and OA spectra are labeled by M_i and $M_{i'}$, respectively, in the order of increasing frequency, and the results are tabulated in Table II. The frequency positions of these spectral features are in good agreement with other published PL and OA spectra. (See, for example, Refs. 3 and 4.)

To show that the energy of the vibronic features in the PL spectra do not depend strongly on excitation energies, we have tabulated the peak energies from spectra excited with 460 nm (column 2) and 330 nm (column 3) in the upper half of Table II. Also, to show that the spectral position of the vibronic features in the OA spectra do not strongly depend on the solvents being used, we list peak energies of the room temperature OA spectra of C_{60} in MCH reported here (column 2) and C_{60} in toluene taken by Leach et al.[3] in column 3 of the lower half of Table II.

In assigning the observed PL and OA features in the C_{60} solution spectra to a particular vibronic transition, we note that a vibronic manifold of states is associated with each of the electronic states (see Table I for the selection rules). The assignments labeled with symbols from $M_{0'}$ to $M_{9'}$ in the observed OA spectrum, are identified as mirror images of the vibronic transitions in the PL spectrum labeled with symbols from M_0 to M_9 (i.e., M_i and $M_{i'}$ involve the same HT active vibrational mode). The vibrational frequencies, ω_{vib} in column 4 of Table II, are calculated as the difference between the observed position of the vibronic feature and the zero-phonon transition energy $E_{0,0'}$ indicated by the solid vertical line in Fig. 3(a). We have chosen $E^{PL}_{0,0'} = 15\,200$ cm^{-1}, and

TABLE II. Vibronic features near the absorption gap in the PL and OA spectra of C_{60} in methylcyclohexane solution (C_{60}/MCH solution), C_{60} single crystal (C_{60}/crystal),[a] and C_{60} solid films (C_{60}/film). Data in the table refer to spectra taken at $\sim$80 K, except the OA spectrum of C_{60} in MCH solution, which was taken at room temperature, and the PL spectrum of C_{60} single crystal, which was taken at 10 K.[a]

Photoluminescence (PL)

i	M_i (cm^{-1})		ω_{vib}[a] (cm^{-1})	ω_{vib}[b] (cm^{-1})	Assignment	C_i[c] (cm^{-1})	$\Delta_C(i)$[d] (cm^{-1})	F_i (cm^{-1})		ω_{vib}[e] (cm^{-1})	Assignment[f]	$\Delta_F(i)$[g] (cm^{-1})
	C_{60}/MCH solution					*C_{60}/crystal*		*C_{60}/film*				
9		12085[h]			$\nu_4(F_{1u})+\nu_7(H_u)$							
8	12455[h]	12438[i]	2745	2858	$2\nu_4(F_{1u})$	12195	260	12225[j]	12177[k]	2775	$\omega_t+2\omega_r$	230
7	13158[h]	13245	2042	2125	$\nu_4(F_{1u})+\nu_3(H_u)$	12959	199	12953[j]	12903[k]	2047	$\omega_t+\omega_r$	205
6	13587[h]	13605[b]	1613	1559	$\nu_7(H_u)$	13408	179	13395[j]	13306[k]	1605		192
5	13793[h]	13810	1407	1429	$\nu_4(F_{1u})$	13652	141	13625[j]	13629[k]	1357	ω_t	168
4	14035[h]	14085[i]	1165	1183, 1117	$\nu_3(F_{1u})+\nu_5(H_u)$	13937	98	13815[j]		1185	$2\omega_r$	220
3	14327[h]	14368[i]	873	840	$\nu_1(H_u)+\nu_1(A_g)$	14218	109					
2	14556[i]	14610[i]	644	696	$\nu_3(H_u)$	14390	166					
1	14804[i]	14804[i]	396	343	$\nu_1(H_u)$	14634	170					
0	15221[i]	15221	-21	0	$^1F_{1g}$ origin							
$E^{PL}_{0,0'}$	15200				$^1F_{1g} \to {}^1A_g$			15000				$\sim$200
Optical absorption (OA)												
$E^{OA}_{0,0'}$	15510				$^1A_g \to {}^1F_{1g}$			15080				$\sim$430
0'		15423[e]		0	$^1F_{1g}$ origin			15020	14870[l]			
1'		15935[e]		343	$\nu_1(H_u)$							
2'	16155	16124[e]	645	696	$\nu_3(H_u)$			15723	15640[l]	643	ω_r	432
3'	16390	16390[e]	880	840	$\nu_1(H_u)+\nu_1(A_g)$							
4'	16717	16720[e]	1207	1183, 1117	$\nu_3(F_{1u})+\nu_5(H_u)$			16313	16260[l]	1233	$2\omega_r$	404
5'	16949	16941[e]	1439	1429	$\nu_4(F_{1u})$			16529	16500[l]	1449	ω_t	420
6'		17242[e]		1559	$\nu_7(H_u)$							
7'	17600	17600[e]	2090	2125	$\nu_4(F_{1u})+\nu_3(H_u)$			17182	17100[l]	2102	$\omega_t+\omega_r$	418
8'	18215	18205[e]	2705	2858	$2\nu_4(F_{1u})$			17762		2792	$\omega_t+2\omega_r$	453
9'	18587	18430[e]	3077	2988	$\nu_4(F_{1u})+\nu_7(H_u)$			18116		3036	$2\omega_t$	471

[a] $\hbar\omega_{vib}$ is the energy of the HT active vibrational modes obtained with respect to band gap $E_{0,0'}$ as indicated.

[b] Results from first-order and second-order Raman and infrared (IR) measurements (Refs. 13 and 14).

[c] C_i represents the single crystal data of Guss et al. (Ref. 17).

[d] $\Delta_C(i) = M_i - C_i$ where M_i and C_i denote the data in the columns 2 and 7, respectively.

[e] OA data of C_{60} in toluene solution at room temperature by Leach et al. (Ref. 3).

[f] ω_r and ω_t refer to characteristic radial and tangential vibrational mode frequencies, respectively, and have values of $\omega_r \cong 640$ cm^{-1}, and $\omega_t \cong 1400$ cm^{-1}.

[g] $\Delta_F(i) = M_i - F_i$ where M_i and F_i denote the data in the columns 9 and 2, respectively.

[h] PL data at $\sim$ 80 K, $\lambda_{ex} = 330$ nm (present work).

[i] PL data at $\sim$ 80 K, $\lambda_{ex} = 460$ nm (present work).

[j] PL data at $\sim$ 80 K, $\lambda_{ex} = 488$ nm (present work).

[k] PL data of C_{60} polycrystalline powder at 5 K, low laser intensity and $\lambda_{ex} = 654$ nm (1.9 eV) by Feldmann et al. (Ref. 30).

[l] OA data of solid C_{60} film on CaF$_2$ substrate at 10 K by Reber et al. (Ref. 18).

$E_{0,0'}^{OA} = 15\,510$ cm^{-1} for the electronic origins for the PL and OA processes in solution. These choices yield values for ω_{vib} (for features M_0 to M_6 in PL and $M_{0'}$ to $M_{6'}$ in OA) in good agreement with first-order Raman[14] and infrared[13] mode frequencies (see column 5, Table II). Our choices of the zero-phonon transition energy $E_{0,0'}$ and the assignments of the PL and OA features agree quite well with those of Negri *et al.*[1] The vibrational frequencies obtained for features labeled M_7 to M_9 in PL, and $M_{7'}$ to $M_{9'}$ in OA, are higher than the highest first-order vibrational mode [i.e., $\omega_{max} \simeq 1578$ cm^{-1} for $H_g(8)$].[14,15] We, therefore, identify these features with HT active overtone ($2\omega_i$) and combination ($\omega_i + \omega_j$) vibrational modes. In general, vibrational modes involved in strong first-order vibronic transitions also participate in strong combination and overtone vibronic transitions. Since the $\nu_4(F_{1u})$ mode is found to be the strongest HT active vibrational mode,[1] we identify features labeled M_7 to M_9 and $M_{7'}$ to $M_{9'}$ with combinations and overtones involving the $\nu_4(F_{1u})$ mode (see Table II). The small differences (~ 50 cm^{-1}) between the vibrational frequencies deduced from the PL and OA spectra relative to values obtained by vibrational spectroscopy are well within experimental error. This error is primarily associated with the broad width of the features seen in the PL and OA spectra. The interaction of the C_{60} molecules with their local environment may also modify the vibrational frequency.[31] Possible reasons for two distinct electronic origins, $E_{0,0'}^{OA}$ for OA and $E_{0,0'}^{PL}$ for PL, include bond relaxation of the molecule in the excited electronic state, a Jahn-Teller effect in the excited state, and the interaction between C_{60} molecules and the solvent. A difference of ~ 300 cm^{-1} between our values for the $E_{0,0'}^{PL}$ and $E_{0,0'}^{OA}$ energies is within the energy range of solute-solvent interactions.[31] Although the transition between zero-vibration vibronic levels (at $E_{0,0'}$) is forbidden by symmetry, a weak peak is seen in the PL spectra [Fig. 3(a)] and also in the OA spectra reported by Leach *et al.*;[3] these transitions are denoted as M_0 and $M_{0'}$ in Table II.

B. Vibronic transitions in C_{60} solid

In Fig. 3(b), we plot the room temperature $T = 300$ K (dotted curves) and 80-K (solid curves) OA and PL spectra of a solid C_{60} film vacuum deposited on a quartz substrate. The spectra were taken on the same spot on the film using the optical arrangement shown in Fig. 1; an excitation wavelength of 488 nm was used for the PL spectrum. It should be noticed that the 80-K OA spectra in the film and in solution have similar features. This suggests the same origin for the transitions in both C_{60} solid films and C_{60} in solution, and is strong evidence for the dominant molecular character of the solid. We, therefore, index (i') the features ($F_{i'}$) in the OA spectrum of the film to correspond to the labels ($M_{i'}$) for the OA spectrum of C_{60}/MCH. The features in the $T = 300$ K OA spectrum of the film are very broad relative to those in the $T = 300$ K C_{60}/MCH solution. However, when the film is cooled to 80-K, the OA spectrum near the optical threshold is remarkably similar to that of the $T = 300$ K

OA spectrum for C_{60} in solution (C_{60}/MCH). It should be noted, however, that the entire 80-K OA spectrum of the C_{60} solid film is redshifted with respect to that of C_{60} in solution. The redshift for each feature in the film OA spectrum is denoted as $\Delta_F(i)$ in the last column in Table II. In the solid state $E_{0,0'}^{OA}$ is lowered by ~ 430 cm^{-1} with respect to that in solution. This shift in $E_{0,0'}^{OA}$ is not due to changes in the vibrational mode frequencies themselves, which are observed to exhibit little change between the solid phase and that of C_{60} in solution.[32] The redshift of the 80-K OA film spectrum relative to the 300-K solution spectrum is four times larger than the ~ 100 cm^{-1} blueshift of this spectrum by lowering the temperature from room temperature to 80 K.

We have labeled the features in the film PL spectrum with the symbols F_4 to F_8 [Fig. 3(b)] to correspond to those features observed in the solution PL spectrum [Fig. 3(a)]. The 80-K film PL spectrum downshifts by ~ 200 cm^{-1} with respect to the 77-K solution PL spectrum. The amount of redshift $\Delta_F(i')$ for each film feature appears in the last column of Table II. Subtracting an average shift $\langle \Delta_F \rangle \sim 200$ cm^{-1} from $E_{0,0'}^{PL} = 15\,200$ cm^{-1} for C_{60} in solution gives $E_{0,0'}^{PL} = 15\,000$ cm^{-1} for the C_{60} solid film. After taking account of this shift in origin, the frequencies of the various HT active modes deduced from the PL data (Table II, column 4) are then in better accord with values obtained from Raman[14] and infrared[13] spectroscopy (column 5). These PL-deduced values for ω_{vib} in the film are close to those deduced from the PL spectrum of C_{60} in solution (see Table II, columns 11 and 4).

Despite the similarities between the film and solution PL and OA spectra, there are three noteworthy differences: (1) the film OA and PL spectra are redshifted in energy with respect to the solution OA and PL spectra, (2) the solution (C_{60}/MCH) features labeled M_0 to M_3 are not observed in the PL spectrum of the film, and (3) the PL features in the solid film [Fig. 3(b)] are broadened considerably with respect to those in the solution [Fig. 3(a)]. This broadening is not simply due to intermolecular C_{60}-C_{60} interactions in the solid state, as can be seen by comparing the 10-K single crystal PL data of Guss *et al.*[17] to that of the 80-K film and the 77-K solution PL data (the features C_i for the single crystal data are labeled similarly to those in solution). If the broadening were due to C_{60}-C_{60} interactions, the single crystal PL spectrum would not be so remarkably similar to that of C_{60} in solution. We have also tabulated the energy of the C_i peaks in column 7 of Table II. However, we do attribute the redshift seen in *both* the film and single crystal PL spectra with respect to the solution PL spectrum to solid state interactions. Since the PL spectrum of the single crystal not only contains most of the features seen in the solution PL spectrum, but also exhibits similar relative intensities of the various features, it is clear that a molecular (HT vibronic) explanation of the structure in the crystal and film PL spectrum must be evoked. Furthermore, the intrinsic intermolecular interaction in fcc C_{60} is, therefore, not responsible for the broadness of the vibronic feature in the film PL spec-

trum. The observed broadening must be identified with grain boundary defects in the film. Consistent with this view is the observation that the PL spectrum of a polycrystalline powder[30,33] also shows similar broad vibronic features.

The energy difference $\Delta_C(i)$ for each feature in the single crystal PL spectra relative to that in C_{60}/MCH (solution) can be found in the eighth column of Table II. By comparing $\Delta_C(i)$ and $\Delta_F(i)$, we see the PL spectra of both single crystal and films downshift by about the same amount relative to the solution spectrum, indicating that the lattice potential introduces the spectral shift. In aromatic, molecular crystals, a spectral shift relative to solution data has been connected with two mechanisms:[31] the *solvent shift* and the *exciton shift*. The *solvent shift* is due to the polarizability of the environment, which is quite different for C_{60} in solution and C_{60} in the pristine solid. The *exciton shift* is due to the electron-hole interaction spread over translationally equivalent molecules. Within a given set of vibronic transitions (e.g., $^1A_g \rightarrow {}^1F_{1g}$), one usually finds that the solvent shift is constant, but the exciton shift is proportional to the intensity of the particular vibronic transition. Unfortunately, due to the large width of the features in the spectra, our experimental uncertainty is about ± 50 cm^{-1}. Therefore, it is not possible to conclude much about the origin of the shift from the i dependence of $\Delta_C(i)$ or $\Delta_F(i)$ found in Table II.

The features F_0 to F_3 are missing in the PL spectrum of the film, but are clearly evident in the PL spectra of the solution C_{60}/MCH and single crystal. The reasons for their absence are not clear, although it must be connected in some way to the interaction of defects with the particular, low frequency (ω_{vib}) vibronic states ($^1A_g; \omega_{vib}$).

It is worth mentioning that the crystal grain size in our solid films is found to be ~ 20 nm, from x-ray data. Thus, many C_{60} molecules are within one or next-neighbor distances of a grain boundary (the C_{60} diameter ~ 1 nm). Grain boundary defects will lower the local symmetry of C_{60} and lift the high degeneracy of the intramolecular modes. Therefore, for molecules located near grain boundaries many more vibrational modes might participate in vibronic transitions. We, therefore, have artificially grouped contributions from radial character vibrational modes ω_r (modes between ~ 200 and ~ 950 cm^{-1}) and from tangential character vibrational modes ω_t (modes between ~ 950 and ~ 1800 cm^{-1}), where $\omega_r \cong 640$ cm^{-1} and $\omega_t \cong 1400$ cm^{-1}, to assign the broad PL and OA features of the thin C_{60} film. These assignments are indicated in column 12 of Table II. Another factor that might contribute to the broadening of the film PL spectrum is the presence of X traps[17] associated with grain boundary defects. An X trap yields a PL spectrum with the same vibronic features as the intrinsic (undisturbed) crystal, but the features are red-shifted by the trap depth ΔE. A range of trap depths ΔE ($25 < \Delta E < 200$ cm^{-1}) would also explain the broadening of the film features we observe.

C. Optical transitions in photopolymerized C_{60}

C_{60} solid films can be readily transformed into a new polymeric phase under irradiation with visible or ul-

traviolet light.[19,20] In this phototransformed phase, it has been proposed that C_{60} molecular shells are coupled together by covalent bonds to form a polymeric solid or "polyfullerene."[20] Some experimental results on photopolymerized C_{60} suggest the formation of four-membered rings located between adjacent C_{60} molecules through "2 + 2" cyclo-addition.[22,24] Recent theoretical calculations on the C_{60} dimer find that a four-membered ring is the lowest energy configuration.[34,35] Photopolymerization by the exciting source may be the cause for the reported[18] problems in the spot-to-spot reproducibility in previous photoluminescence studies of C_{60}.

In Fig. 4(a) we compare the room temperature absorbance [$\mathcal{A} = -\log_{10}(\mathcal{T})$, $\mathcal{T} = $ transmission] of a C_{60} film ($d \sim 500$ Å) on a Suprasil substrate in the pristine (solid curve) and phototransformed (dashed curve) phases. Earlier, we have identified the four prominent absorption peaks at ~ 2.7, 3.6, 4.7, and 5.6 eV for the pristine phase with dipole-allowed electronic transitions.[8] Significant oscillator strength exists for these transitions in the absence of an electron-vibration interaction. The peak at ~ 2.7 eV has been identified[8] with two groups of transitions. The first group is between the HOMO (h_u-derived states) to LUMO+1 (t_{1g}-derived states). For this discussion we have used one-electron state symmetry labels (i.e., h_u, t_{1u}, g_g, etc.) to identify initial and fi-
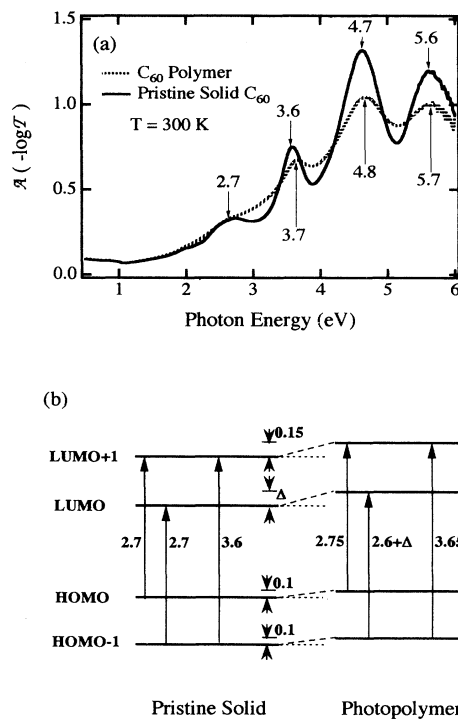
FIG. 4. (a) Optical absorbance $\mathcal{A}$ for pristine and photopolymerized C_{60} solid films ($d \sim 500$ Å) on a Suprasil (fused silica) substrate in the photon energy range 0.5–6.0 eV. The same C_{60} film was used for both spectra. (b) Schematic electronic states and optical transitions of pristine and photopolymerized solid C_{60}. The numbers denote the transition energies (in eV) at the center of the optical band.

nal states. For dipole-allowed transitions, this description of the electronic states is sufficient, and furthermore conforms to many of the theoretical calculations available in the literature. The second group of transitions contributing to the 2.7 eV peak involve the HOMO-1 (g_g and h_g) to LUMO (t_{1u}) transitions. The peak at ~3.6 eV has been identified with HOMO-1 (g_g, h_g) to LUMO+1 (t_{1g}) transitions.[8] HOMO and HOMO-1 denote the highest and the next-highest occupied molecular states, respectively, whereas LUMO and LUMO+1 denote the lowest and next-highest, unoccupied molecular states, respectively. It should be noticed that the 3.6 eV band has been assigned to transitions between bands derived from gerade-symmetry orbitals. Although vertical (wave-vector conserving) transitions between bands derived from these states are forbidden at the center of the Brillouin zone (Γ point), vertical transitions between states in these bands at other points throughout the zone are allowed, however,[6] the intensities are wave-vector dependent.

After photopolymerization, these optical transitions form optical bands that are noticeably broadened [Fig. 4(a)]. We attribute this broadening to a random photochemical cross linking of C_{60} molecules, i.e., inhomogeneous broadening. Cross linking the molecular shells completely removes the degeneracies of the electronic energy levels in the C_{60} monomers. Also, the phototransformation generates a distribution of C_{60} oligomeric units. Both of these changes in the system should contribute to line broadening. We found that the width of the peak at ~3.6 eV in the "polyfullerene" phase is ~0.3 eV wider than that in the pristine phase by fitting Lorentz oscillator functions to the absorption spectra. This ~0.3 eV broadening is consistent with the results of photoelectron spectroscopy[25] where the electronic energy levels (HOMO and HOMO-1 states) in the photoemission spectra of photopolymerized C_{60} were found to be ~0.1–0.15 eV wider than those in pristine C_{60}. We expect the LUMO+1 states to be broadened by about the same amount as the HOMO states.

In addition to the photoinduced broadening of the absorption bands in polyfullerene, the peaks at ~3.6, 4.7, and 5.6 eV in pristine solid C_{60} are noticeably blueshifted in the polymer. The ~2.7-eV band in the polymer is too broad to locate its center. To visualize the effect of photopolymerization on the lowest energy states, we plot a schematic diagram in Fig. 4(b) of the electronic energy levels for the pristine and phototransformed material. The solid thick horizontal lines in the figure represent the peak positions of the calculated Gaussian density of state for the corresponding band of electronic states.[6] Allowed optical transitions and the transition energies (in eV) are shown in the figure. To explain the OA blueshift upon phototransformation, and to be consistent with the photoemission data on the photopolymer,[25] the electronic levels of the phototransformed C_{60} are upshifted with respect to the electronic levels of pristine C_{60}. In the figure, Δ is an energy shift of the LUMO level in the phototransformed phase which can be estimated from our data. Since the optical band in the phototransformed C_{60} solid that is assigned to electronic transitions be-

tween the HOMO-1 and LUMO+1 states (at ~3.7 eV) is blueshifted by ~0.05 eV, the LUMO+1 states are upshifted by ~0.15 eV to be consistent with the photoemission results.[25] If the LUMO state is not also upshifted by ~0.15 eV (i.e., $\Delta \neq$ ~0.15 eV), the energies of the HOMO $\rightarrow$ LUMO+1 and HOMO-1 $\rightarrow$ LUMO transitions will be different [see Fig. 4(b)], and the peak at ~2.7 eV in the pristine C_{60} spectrum would split into two poorly resolved peaks in the phototransformed C_{60} spectrum. Since we see no evidence for an unresolved doublet at ~3.7 eV, we assume that $\Delta \sim$ 0.1–0.2 eV.

In Fig. 5, we display the PL spectra at 80 K for the same C_{60} film on a Suprasil fused silica substrate before (solid curve) and after (dashed curve) the phototransformation. A ~330-cm^{-1} spectral redshift and peak broadening of the vibronic transitions in the whole spectrum is observed upon phototransformation. Because of the similarity of the phototransformed spectrum to that of monomeric C_{60}, the features in the photopolymerized spectrum are still closely related to those observed in Fig. 3 for the C_{60} film prior to phototransformation. The redshift of the PL features for the polymer relative to the peak energies for the pristine film is consistent with the luminescence redshifts observed with oligomerization (i.e., monomer $\rightarrow$ dimer, dimer $\rightarrow$ trimer, etc.), such as is observed in the helicene series and in polyacenes.[31] Furthermore, it can be seen that the two predominant peaks at ~11 895 cm^{-1} and 13 292 cm^{-1} and the shoulders in the spectrum of the phototransformed sample are slightly broadened compared to those (at 12 225 cm^{-1} and 13 625 cm^{-1}) in the pristine spectrum. This broadening effect is consistent with the lifting of degeneracies in the vibrational modes as seen in Raman and IR vibrational spectroscopy of the photopolymer,[20] and is also consistent with the inhomogeneous broadening discussed above in connection with the OA spectrum of the polymer.
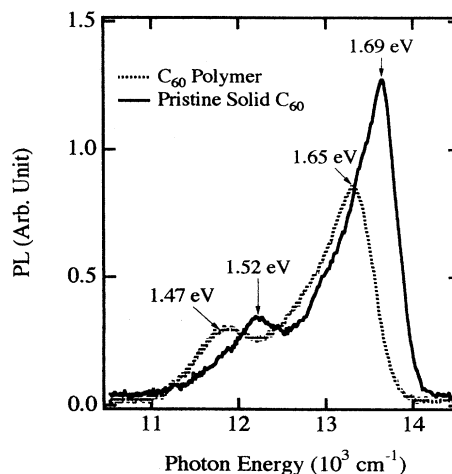

FIG. 5. Photoluminescence spectra at 80 K for pristine (solid line) and phototransformed (dotted line) C_{60} film (~4500 Å thick) on a Suprasil fused silica substrate. The same C_{60} film was used for both spectra.

IV. CONCLUSIONS

Vibronic transitions successfully explain our experimental OA and PL spectra of C_{60} near the threshold for electronic absorption, and provide a natural explanation for the oscillator strength observed between the ground state ^1A_g and gerade excited electronic states near the HOMO-LUMO gap. It is concluded that the optical transitions that occur in this energy range in C_{60} solutions and in the solid state have the same origin, i.e., the coupling of the excited singlet $^1F_{1g}$ state and the singlet ground state ^1A_g to HT active vibrational modes. The HT active intramolecular modes at high frequency (~ 1400 cm^{-1}) make strong contributions to both the PL and OA spectra of C_{60} in solution and in solid C_{60}. The difference in the C_{60}-solvent and C_{60}-C_{60} interactions is identified as the origin of the OA spectral redshift. The considerable broadening of the narrow vibronic structure in the PL and OA spectra of C_{60} in solution is attributed to grain boundary defects in C_{60} solid films. X traps may also be responsible for this broadening.

In the photopolymerized C_{60} solid films, the covalent C-C bonds between C_{60} shells perturb the icosahedral (I_h) shell symmetry and lift the degeneracy of the electronic levels and vibrational modes of the C_{60} molecules. This is proposed to activate more vibronic transitions and broaden the PL and OA features as observed. Inhomogeneous broadening due to the distribution of photoproduced oligomers also contributes to the linewidth, and may well be the dominant mechanism for line broadening. Level shifting of the states near the Fermi level of the poly-fullerene solid gives rise to a red shift in the PL vibronic spectrum and a blueshift of the dipole-allowed optical bands in the UV-vis region.

* Present address: CSM Ltd., 2 Science Park Drive, Singapore Science Park, Singapore 0511.

† Author to whom correspondence should be addressed. Also at Center for Applied Energy Research, 3572 Iron Works Pike, Lexington, KY 40511-8433.

‡ Present address: Harry Reid Center for Environmental Study, University of Nevada, Las Vegas, NV 89154-4099.

[1] F. Negri, G. Orlandi, and F. Zerbetto, J. Chem. Phys. **97**, 6496 (1992).

[2] K. Yabana and G. Bertsch, Chem. Phys. Lett. **197**, 32 (1992).

[3] S. Leach, M. Vervloet, A. Després, E. Bréheret, J. P. Hare, T. J. Dennis, H. W. Kroto, R. Taylor, and D. R. M. Walton, Chem. Phys. **160**, 451 (1992).

[4] Ying Wang, J. Phys. Chem. **96**, 764 (1992).

[5] Riichiro Saito, G. Dresselhaus, and M. S. Dresselhaus, Chem. Phys. Lett. **210**, 159 (1993).

[6] W. Y. Ching, Ming-Zhu Huang, Yong-Nian Xu, W. G. Harter, and F. T. Chan, Phys. Rev. Lett. **67**, 2045 (1991).

[7] S. G. Louie (private communication).

[8] Ying Wang, J. M. Holden, A. M. Rao, Wen-Tse Lee, G. T. Hager, X. X. Bi, S. L. Ren, G. W. Lehman, G. T. Hager, and P. C. Eklund, Phys. Rev. B **45**, 14 396 (1992).

[9] P. C. Eklund, A. M. Rao, Y. Wang, P. Zhou, K. A. Wang, J. M. Holden, M. S. Dresselhaus, and G. Dresselhaus, in *Thin Films*, edited by D. M. Gruen (World Scientific Publishing Co. Ltd., Singapore, in press).

[10] P. J. Benning, J. L. Martins, J. H. Weaver, L. P. F. Chibante, and R. E. Smalley, Science **252**, 1417 (1991).

[11] T. Takahashi, S. Suzuki, T. Morikawa, H. Katayama-Yoshida, S. Hasegawa, H. Inokuchi, K. Seki, K. Kikuchi, S. Suzuki, K. Ikemoto, and Y. Achiba, Phys. Rev. Lett. **68**, 1232 (1992).

[12] R. W. Lof, M. A. van Veenendaal, B. Koopmans, H. T. Jonkman, and G. A. Sawatzky, Phys. Rev. Lett. **68**, 3924 (1992).

[13] K. A. Wang, A. M. Rao, P. C. Eklund, M. S. Dresselhaus, and G. Dresselhaus, Phys. Rev. B **48**, 11375 (1993).

[14] Z. H. Dong, P. Zhou, J. M. Holden, P. C. Eklund, M. S. Dresselhaus, and G. Dresselhaus, Phys. Rev. B **48**, 2862 (1993).

[15] S. Saito and A. Oshiyama, Phys. Rev. Lett. **66**, 2637 (1991).

[16] K. Harigaya (private communication).

[17] W. Guss, J. Feldman, E. O. Göbel, C. Taliani, H. W. Müller, P. Häussler, and H. U. ter Meer, Phys. Rev. Lett. **72**, 2644 (1994).

[18] C. Reber, L. Yee, J. McKiernan, J. I. Zink, R. S. Williams, W. M. Tong, D. A. A. Ohlberg, R. L. Whetten, and F. Diederich, J. Phys. Chem. **95**, 2127 (1991).

[19] P. Zhou, A. M. Rao, K. A. Wang, J. D. Robertson, C. Eloi, M. S. Meier, S. L. Ren, X. X. Bi, and P. C. Eklund, Appl. Phys. Lett. **60**, 2871 (1992).

[20] A. M. Rao, P. Zhou, K.-A. Wang, G. T. Hager, J. M. Holden, Ying Wang, W. T. Lee, Xiang-Xin Bi, P. C. Eklund, D. S. Cornett, M. A. Duncan, and I. J. Amster, Science **259**, 955 (1993).

[21] D. S. Cornett, I. J. Amster, M. A. Duncan, A. M. Rao, and P. C. Eklund, J. Phys. Chem. **97**, 5036 (1993).

[22] P. Zhou, Z. H. Dong, A. M. Rao, and P. C. Eklund, Chem. Phys. Lett. **211**, 337 (1993).

[23] Y. Wang, J. M. Holden, Z. H. Dong, X. X. Bi, and P. C. Eklund, Chem. Phys. Lett. **211**, 341 (1993).

[24] Ying Wang, J. M. Holden, X. X. Bi, and P. C. Eklund, Chem. Phys. Lett. **217**, 413 (1994).

[25] A. Ito, T. Morihawa, and T. Takahashi, Chem. Phys. Lett. **211**, 333 (1993).

[26] P. C. Eklund, Ping Zhou, Kai-An Wang, G. Dresselhaus, and M. S. Dresselhaus, J. Phys. Chem. Solids **53**, 1391 (1992).

[27] M.S. Meier and J.P. Selegue, J. Org. Chem. **57**, 1925 (1992).

[28] F. Negri, G. Orlandi, and F. Zerbetto, Chem. Phys. Lett. **144**, 31 (1988).

[29] Z. Gasyna, P. N. Schatz, J. P. Hare, T. J. Dennis, H. W. Kroto, R. Taylor, and D. R. M. Walton, Chem. Phys. Lett. **183**, 283 (1991).

[30] J. Feldmann, R. Fischer, E.O. Gobel, and S. Schmitt-Rink, Phys. Status Solidi B **173**, 339 (1992).

[31] J. B. Birks, *Photophysics of Aromatic Molecules* (Wiley and Sons, London, 1970).

[32] B. Chase, N. Herron, and E. Holler, J. Phys. Chem. **96**, 4262 (1992).

[33] J.L. Sauvajol, Z. Hricha, N. Coustel, A. Zahab, and R. Aznar, J. Phys. Condens. Matter **5**, 2045 (1993).

[34] M. Menon, K. R. Subbaswamy, and M. Sawtarie, Phys. Rev. **49**, 13 966 (1994).

[35] D. L. Strout, R.L. Murry, C. Xu, W.C. Eckhoff, G.K. Odom, and G. E. Scuseria, Chem. Phys. Lett. **214**, 576 (1993).